Applied Physics Letters

In situ Raman scattering studies of pressure-temperature phase diagrams in antiferroelectric xCaSnO$_3$-modified NaNbO$_3$ ceramics

Cite as: Appl. Phys. Lett. **119**, 132905 (2021); https://doi.org/10.1063/5.0060874
Submitted: 23 June 2021 . Accepted: 16 September 2021 . Published Online: 28 September 2021

Yan Ye (叶艳), **Anyang Cui** (崔安阳), **Lichen Gao** (高立宸), **et al.**

Applied Physics Letters ARTICLE scitation.org/journal/apl

In situ Raman scattering studies of pressure-temperature phase diagrams in antiferroelectric xCaSnO$_3$-modified NaNbO$_3$ ceramics

Cite as: Appl. Phys. Lett. **119**, 132905 (2021); doi: 10.1063/5.0060874
Submitted: 23 June 2021 · Accepted: 16 September 2021 ·
Published Online: 28 September 2021

Yan Ye (叶艳),[1] Anyang Cui (崔安阳),[1] Lichen Gao (高立宸),[1] Kai Jiang (姜凯),[1] Liangqing Zhu (朱亮清),[1] Jinzhong Zhang (张金中),[1] Liyan Shang (商丽燕),[1] Yawei Li (李亚巍),[1] Genshui Wang (王根水),[2] Xianlin Dong (董显林),[2] Zhigao Hu (胡志高),[1,3,4,a)] and Junhao Chu (褚君浩)[1,3,4]

AFFILIATIONS

[1]Technical Center for Multifunctional Magneto-Optical Spectroscopy (Shanghai), Engineering Research Center of Nanophotonics and Advanced Instrument (Ministry of Education), Department of Materials, School of Physics and Electronic Science, East China Normal University, Shanghai 200241, China

[2]Key Laboratory of Inorganic Functional Materials and Devices, Shanghai Institute of Ceramics, Chinese Academy of Sciences, Shanghai 200050, China

[3]Collaborative Innovation Center of Extreme Optics, Shanxi University, Taiyuan, Shanxi 030006, China

[4]Shanghai Institute of Intelligent Electronics and Systems, Fudan University, Shanghai 200433, China

[a)]Author to whom correspondence should be addressed: zghu@ee.ecnu.edu.cn

ABSTRACT

As one of the classic antiferroelectrics, high complexity of a NaNbO$_3$ structure sequence attracts great attention in the ferroelectric physics field. Here, temperature-pressure phase diagrams as a function of a CaSnO$_3$ content for antiferroelectric (1-x)NaNbO$_3$-xCaSnO$_3$ ceramics have been improved by Raman spectroscopy. We clarify structural order of phase transitions on CaSnO$_3$-modified NaNbO$_3$ ceramics within the temperature range of 80–840 K by discussing the anomalies of lattice and phonon dynamics. The doping effect of CaSnO$_3$ on the P-R phase transition has been summarized from the decreased critical temperature from 660 to 580 K. The intermediate phase at 480 K was recognized as an incommensurate phase. In addition, the anomalous pressure with respect to phonon frequency at the stress field of 0–25 GPa also provides the evidence of structural transformations at 6.55 and 10.05 GPa. Upon increasing the CaSnO$_3$ content, phase transition moves to a lower pressure range. This work would provide the powerful supplement of phase transitions for the broad NaNbO$_3$-based crystalline family with Raman scattering.

Since the concept of antiferroelectricity was originally proposed by Kittel,[1] state-of-the-art antiferroelectric (AFE) functionality has greatly supported the rapid development of high-energy capacitors, electrocaloric refrigerators, and nonvolatile random access memories.[2–5] AFE is intrinsically derived from the opposite-oriented spontaneous polarizations between adjacent unit cells. Except for the archetype AFE PbZrO$_3$-based ceramics, lead-free NaNbO$_3$ (NN) is regarded as one of the well-documented lead-free AFE materials with high energy storage density.[6–8] It exhibits the orthorhombic structure with *Pbma* symmetry at room temperature, also described as the AFE P phase in Glazer's notation.[9] A polycrystalline NaNbO$_3$ system with equal free energy allows the coexistence of a ferroelectric (FE) orthorhombic Q phase ($P2_1ma$) and the AFE P phase.[10,11] Hence, plenty of attempts have focused on the stability of the AFE phase in NN-based ceramics. The proper structure modification of a chemical component has become an effective strategy to improve their functional performance.[12–14] One typical case shows that the introduction of CaSnO$_3$ leads to the descent of tolerance factor, which would enhance the antiferroelectricity of NN-based ceramics.[14]

NaNbO$_3$ holds a complex phase diagram, undergoing a variety of phase transitions including antiferrodistortion and ferrodistortion under the thermal and stress fields. It is commonly recognized that

$NaNbO_3$ goes through six sequent transition processes with seven phases on cooling, following cubic U phase (*Pm3m*) → tetragonal T_2 phase (*P4/mbm*, 913 K) → orthorhombic T_1 phase (*Ccmm*, 848 K) → orthorhombic S phase (*Pnmm*, 793 K) → orthorhombic R phase (*Pmnm*, 753 K) → orthorhombic P phase (*Pbma*, 633 K) → rhombohedral N phase (*R3c*, 173 K).[15–18] Additionally, it has been reported that $NaNbO_3$ undergoes two or three successive structural transformations with external stress manipulation in the range of 0–15 GPa.[19–22] However, the doping effect on structural distortion and transition orders of $x CaSnO_3$-modified NN ceramics has not been studied yet. Consequently, it is necessary to carry out a comprehensive investigation about the structure evolution with the doping, temperature, and pressure. This would play a significant role in developing the stability of structure and functionality, as well as exploring the fundamental mechanism of a potential phase transition.

Raman scattering spectroscopy becomes an effective and nondestructive technique to analyze structure properties relating to the details of a polycrystalline state. It provides versatile evidence for identifying chemical composition, crystallinity, phase transformation, and the evolution of the lattice (symmetry, lattice volume, and strain) by regulating external fields such as electric field, temperature, and pressure.[23–26] Therefore, the study of Raman scattering is expected to systematically understand the phase and phonon transition behaviors.

In this Letter, we performed experimental investigations comprehensively for exploring the structure properties and phase transition sequences in antiferroelectric $NaNbO_3$ ceramics. These experiments were manipulated with the internal factor of various $CaSnO_3$ contents as well as the external fields (temperature and pressure). Raman spectroscopy is applied to reveal the multi-field-driven structural transition by specifying thermal/stress-induced phonon dynamics. The present results would greatly promote the understanding of polycrystalline structure details under the doping, stress, and thermal manipulations in $(1-x)NaNbO_3$-$xCaSnO_3$, which is directly correlated with the significant AFE property and the deriving high-power energy applications.

$(1-x)NaNbO_3$-$xCaSnO_3$ (NNCS100*x*, $x = 0.00$, 0.01, 0.02, 0.03, and 0.04) ceramic samples were prepared by the conventional solid-state relation, which could be found in Ref. 14. Raman scattering measurements were performed on Jobin-Yvon LabRAN HR evolution with a 532-nm exciting laser. Temperature-dependent Raman characterizations were performed by a Linkam THMSE 600 heating/cooling stage. All temperature-dependent Raman spectra were eliminated by the contribution of the Bose–Einstein temperature factor. Pressure-dependent Raman characterizations were performed via a diamond anvil cell (DAC) at room temperature. The diameter of diamond culets in DAC is 300 μm. The tungsten gasket has a hole with a diameter of 100 μm. The pressure-transmitting medium is silicone oil. The ruby luminescence method was used to calibrate the pressure.[27]

Figure 1(a) illustrates Raman spectra from $NaNbO_3$ ceramics with various $CaSnO_3$-doping contents at room temperature. It can be found that NNCS100*x* ceramics stabilize in the orthorhombic structure (space group: *Pbma*, D_{2h}^{11}), which can be referred to the XRD patterns in Ref. 14. According to group theory prediction, it has 60 Raman-active modes, which could also be assigned to *Pbcm* equivalently.[28,29] These Raman modes belong to $15A_g + 17B_{1g} + 15B_{2g} + 13B_{3g}$, given by the irreducible representation at the center of the Brillouin zone.[29] However, only distinguished 19 peaks can be detected owing to the weak intensity between some modes and accidental degeneracy. As

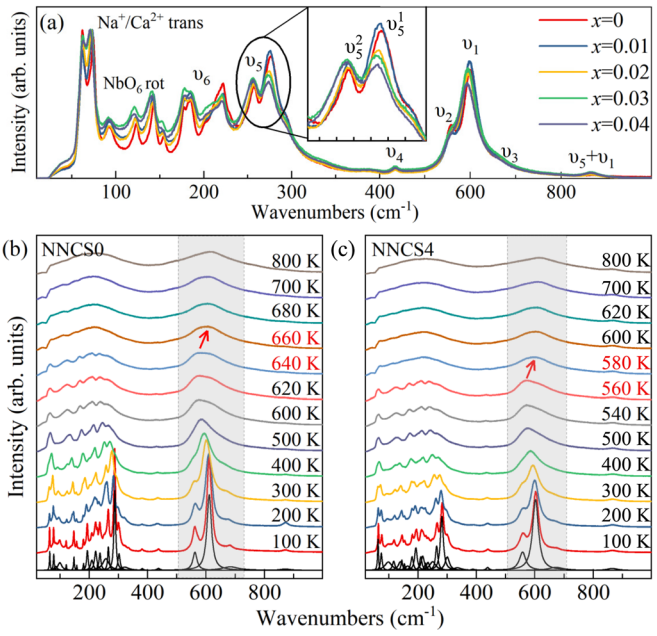

FIG. 1. Raman spectra of (a) five NNCS100*x* ceramics at room temperature and the temperature dependence on (b) NNCS0 and (c) NNCS4 ceramics. The corresponding multi-Lorentz peak fitting at 100 K is shown at bottom.

shown in Fig. 1(a), some peaks broaden as the $CaSnO_3$ content increases, as a result of the change in lattice distortion and internal stress. All modes slightly move to lower frequencies, due to the replacement with heavier doping atoms. There is no obvious variation among the spectra, illustrating that the addition of $CaSnO_3$ does not lead to phase transition. The vibrational modes below 160 cm^{-1} are derived from Na^+ or Ca^{2+} translation and NbO_6 octahedral rotation. The modes above 160 cm^{-1} are primarily related to the internal vibration of NbO_6 octahedra. The phonon modes associated with O-Nb-O bending vibration are mainly located at the range of 160–400 cm^{-1} (ν_5 and ν_6). The modes at 400–750 cm^{-1} are dominated by O-Nb-O stretching involving ν_1, ν_2, ν_3, and ν_4. Phonons around 870 cm^{-1} are assigned to the irreducible coupling mode of $\nu_1 + \nu_5$. With the increasing introduction of the $CaSnO_3$ dopant, the peak intensity of vibrational modes below 160 cm^{-1} gradually increases. It suggests that the antiferrodistortion relative to Na^+/Ca^{2+} translation and NbO_6 octahedral rotation becomes more distinct. Simultaneously, as the content of $CaSnO_3$ increases, the weaker average polarizability of B-site ions leads to lower frequencies of the O-Nb-O stretching ν_1 mode. In addition, the relative peak intensity of some specific modes, such as Na^+ or Ca^{2+} translation and ν_5, can be varied from different contents of $CaSnO_3$. In detail, the split peaks at 256 (ν_5^2) and 278 (ν_5^1) cm^{-1} of the ν_5 mode present $CaSnO_3$-content dependence of the relative intensity, as shown in the inset of Fig. 1(a). Obviously, the bending vibration of the ν_5 mode is connected with not only the displacement of B-site ions and its polarizability but also the distortion of BO_6 octahedra. Hence, the decrease in the relative intensity would be a sign for the enhanced antiferroelectricity on higher $CaSnO_3$ contents for the same phase.

To give the specific discussion on the field-dependent phonon dynamics, the pure $NaNbO_3$ and the heavy doping one (NNCS4,

$x = 0.04$) are selected as the representatives due to the clear variations between the lattice characteristics. First of all, temperature-dependent Raman spectra have been recorded and exhibit lattice and phonon thermodynamics of NNCS0 and NNCS4, as shown in Figs. 1(b) and 1(c). The fitted lines for identifying vibrational modes are obtained at 100 K by Lorentzian-shaped deconvolution with the damped harmonic oscillator model. Owing to the thermal expansion effect caused by the heating, almost all scattering peaks gradually shift to a lower frequency. Two bands reflecting Na^+/Ca^{2+} translation at 62 and 73 cm^{-1} merge into one with increasing the temperature. Peaks between 100 and 400 cm^{-1} gradually weaken and eventually merge into the background signals, indicating the decrease in the structural distortion and improvement in the lattice symmetry. All phase transitions of the modified $NaNbO_3$ ceramics are diffused, due to phase coexistence, and present slight deviation at a temperature scale, as compared with $NaNbO_3$ single crystals.[23] Distinct spectral changes at 640–660 K for NNCS0 and 560–580 K for NNCS4 are associated with the structural transition from the orthorhombic P phase to the R phase, respectively.

In order to recognize the potential phase transitions during the heating process, five typical vibrational modes are selected for NNCS0 in Figs. 2(a)–2(e) and for NNCS4 in Figs. 2(f)–2(j). The magnitude of frequency shifts for various modes is distinguished from each other. The Na^+/Ca^{2+} translational mode located at about 76 cm^{-1} shifts about 10 cm^{-1}, which is less than the shift of any modes related to NbO_6 octahedral vibrations in Fig. 2. It indicates that the translation behavior of Na^+/Ca^{2+} ions has weaker sensitivity to temperature than the octahedral vibration of NbO_6 does. Moreover, abnormal behaviors could be observed for most of vibrational modes around the critical temperatures. After excluding the contributions of lattice expansion and phonon coupling, the abnormal frequency shift would be ascribed to the intrinsic structure variations.[25] As for NNCS0, structural transitions on heating occur at 220 and 660 K, associating with N-P and P-R phase transformations, respectively. The structure transition into the R phase is accompanied by the displacement of the B-site Nb atom. Particularly, we also observe a hysteresis about 50 K for R-P transition on cooling, confirming the existence of first-order phase transition. Although both P and R phases have orthorhombic symmetry, the atomic arrangement of the R phase is fundamentally different from that of the P phase. Specifically, the P phase in a rhombic orientation has tilt systems of pairs of $a^-b^+a^-$ layers alternating with pairs of $a^-b^-a^-$ layers, while the R phase in a parallel orientation has pairs of $a^-b^+c^+$ layers alternating with single $a^-b^0c^+$ layers.[9] Interestingly, the phonon modes of ν_1 and ν_5 related to O-Nb-O vibration present abnormal shifts near 480 K as well, where the sudden increase in the frequency may be attributed to the decreasing of corresponding bonds. Compared with the previous reports, it suggests that there is a phase transition from the P phase to the incommensurate (INC) phase.[23,30,31] As a disordered phase between the other two phases, the INC phase has been confirmed to link with rotations of NbO_6 octahedra modulated along the b-direction.[23] Additionally, there is the invar effect in the INC phase described as being resulted from the competition between thermal vibration and displacement of static atoms. As shown in Figs. 2(f)–2(j), the temperature of each phase transition for NNSC4 is about 200, 460, and 580 K, respectively. Therefore, a preliminary conclusion could be drawn that the phase transition temperature decreases with the $CaSnO_3$ content increases.

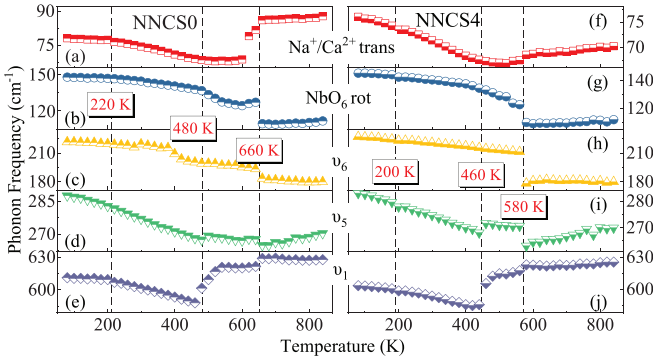

FIG. 2. Center frequency evolutions of main typical Raman-active modes under the heating process (80–840 K) for (a)–(e) NNCS0 and (f)–(j) NNCS4 ceramics. The dashed lines mark the critical temperature of adjacent phases.

In addition to temperature, hydrostatic pressure manipulation is another fundamental condition for more completely understand the structure property with the $CaSnO_3$ doping effect on NNCS100x ceramics. Figures 3(a) and 3(b) show pressure dependence of Raman spectra from NNCS0 and NNCS4 ceramics at room temperature. Vibrational modes including the translational modes, NbO_6 octahedral rotation, and ν_6, ν_5, and ν_4 show high sensitivity to the lattice volume or pressure variation.[19] Below 6.55 GPa, the spectra evolve continuous changes. It can be seen that the intensity of phonons located at 10–400 cm^{-1} gradually reduces. Then, the scattering peaks of ν_6 and ν_5 modes with low intensity merge into the main broad peaks as the pressure reaches 6.55 GPa for NNCS0. However, the interaction between Na^+ cations and NbO_6 octahedral units strengthens at low pressure ranges. Subsequently, the lattice structure has a high degree of disorder, especially for Na^+ ion, which is responsible for the broadening of peaks. Meanwhile, NbO_6 octahedra performs the growing distortion under higher pressure, as a result of the volume shrinkage with the pressure. Hence, additional changes from Raman spectra occur when the pressure holds on more than 10 GPa. Because Raman spectra are extremely sensitive to the lattice structure, the band mutations observed at 6.55 and 10.05 GPa for NNCS0 indicate two structural phase transformation under high pressures (HPs), noted as HP-I and HP-II phases, respectively. The transition around 6.55 GPa is mainly attributed to lattice vibration and the interaction between Na^+ and NbO_6 resulting from the internal vibration of NbO_6. On the other hand, the lattice beyond 10.05 GPa belongs to a paraelectric orthorhombic phase with space group $Pbnm$.[20,21] It is worth noting that phonon dynamics at the high pressure phase is not similar to those at high or low temperature phases. Thus, we would consider that the high pressure phase cannot be obtained at ambient pressures with various temperatures.

Phonon frequencies of vibrational modes with respect to pressure for NNCS0 and NNCS4 are plotted in Figs. 3(c) and 3(d). Frequency evolution generally presents a blue-shift trend with increasing the pressure. For instance, the frequencies of vibrational behavior of Nb-O stretching (500–750 cm^{-1}) increase with the pressure, implying shortening of the Nb–O bond length. As shown in Fig. 3(c), the abnormal shift of phonon frequencies could be probed at 6.55 GPa. The frequency shift as a function of pressure presents various rates (or slope) within different pressure ranges, reflecting the distinct structure. Slopes of pressure dependence change abruptly around 6.55 and

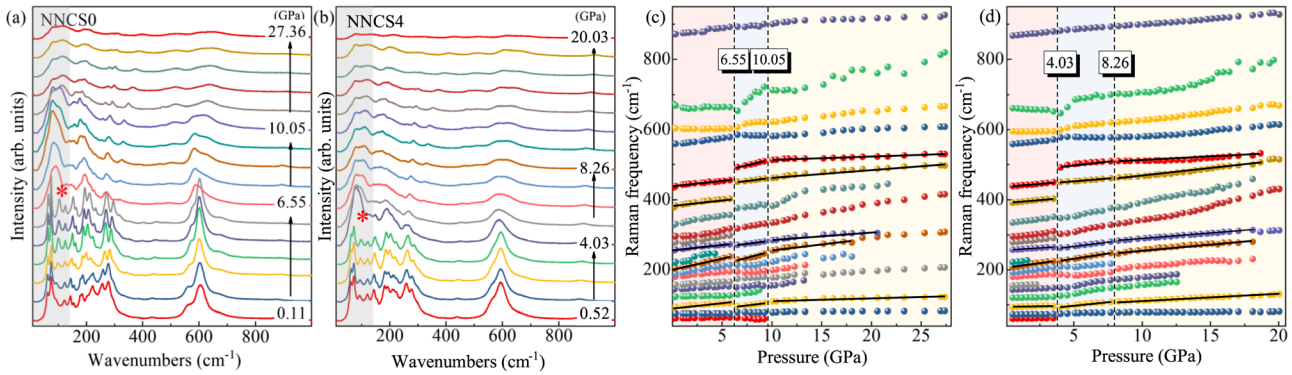

FIG. 3. The pressure dependence of Raman spectra on (a) NNCS0 and (b) NNCS4 ceramics. Center frequency evolution of Raman bands under an external stress field for (b) NNCS0 and (c) NNCS4 ceramics. The dashed lines mark the critical pressure of the adjacent phase.

10.05 GPa for most of modes for NNCS0 ceramics. It is related to the increased repulsive force after completion of rotational rearrangement and Na^+-NbO_6^- touching. The NbO_6 rotation mode disappears under higher pressures, owing to the mutual hindrance of atomic motions. Therefore, the abnormal evolution of phonon behaviors would illustrate the critical phenomenon near phase transition. The pressure dependence of the phonon frequency for the NNCS4 sample shows the similar trends, revealing the critical pressures of around 4.03 and 8.26 GPa, as shown in Fig. 3(d).

To further explore the compressibility of the lattice at different high-pressure phases, frequencies of main vibrational modes as a function of pressure have been investigated in detail. The linear plot of the frequency against pressure is generally expressed as the pressure coefficient. The calculated pressure coefficients of υ_5 and υ_6 modes of NbO_6 octahedra are summarized in Table I, where υ_5 and υ_6 modes present high pressure-sensitivity in the stress field. As for the HP-I phase, the pressure coefficient is larger than those for other phases. The stress-induced displacement of Na^+ ions in the HP-I phase leads to the strength of NbO_6 internal vibration. The pressure coefficient for the HP-II phase is small, because octahedral rotation has a weak contribution to the HP-II phase transformation with the closed packing of Na^+-NbO_6^- ions.[22] Furthermore, the pressure coefficient for the υ_6 mode is generally larger than that for the υ_5 mode. Therefore, we would claim that the υ_6 mode is more sensitive with the pressure than the υ_5 mode, although both modes are derived from O-Nb-O bending vibration.

TABLE I. The pressure coefficient of υ_6 and υ_5 modes for NNCS100*x* ceramics in different high-pressure phases, where the center frequency (cm^{-1}) is confined at ambient pressures. The estimated error bar is obtained by considering high reliability of the fitting parameters.

Sample	Frequency (cm^{-1})	P phase	HP-I phase	HP-II phase
NNCS0	201.2 υ_6	2.85 ± 0.01	3.29 ± 0.03	3.52 ± 0.02
NNCS1	204.4 υ_6	3.39 ± 0.01	5.56 ± 0.02	1.67 ± 0.04
NNCS2	212.8 υ_6	2.89 ± 0.01	5.98 ± 0.02	1.65 ± 0.01
NNCS3	211.1 υ_6	2.21 ± 0.01	5.56 ± 0.02	2.78 ± 0.07
NNCS4	210.8 υ_6	2.19 ± 0.02	2.65 ± 0.01	1.45 ± 0.04
NNCS0	255.7 υ_5	1.09 ± 0.01	2.14 ± 0.01	1.60 ± 0.01
NNCS1	255.6 υ_5	1.41 ± 0.03	1.91 ± 0.01	2.75 ± 0.01
NNCS2	255.1 υ_5	1.26 ± 0.01	2.34 ± 0.01	1.50 ± 0.01
NNCS3	254.5 υ_5	1.14 ± 0.01	0.95 ± 0.01	1.95 ± 0.02
NNCS4	254.4 υ_5	0.95 ± 0.01	2.14 ± 0.01	1.21 ± 0.03

On the basis of the achieved experimental results, the phase diagrams of $CaSnO_3$-content dependent $NaNbO_3$ ceramics under temperature and pressure effects have been concluded in Fig. 4. NNCS100*x* ceramics undergo the successive phase transformations within the temperature range as following: N phase → P phase → INC phase → R phase. The present phase transition order of NNCS100*x* ceramics may result from the competitive lattice instabilities at different points of the Brillouin zone.[23] Additionally, the sequent structural phase transition of $NaNbO_3$-based ceramics is related to the off-centering displacement of Nb in the NbO_6 group and the tilt of octahedra. The transformation temperature increases upon the introduction of the $CaSnO_3$ content at first and then decreases as the $CaSnO_3$ content increases. During the heating process, the FE to AFE transition for NNCS100*x* ceramics has been extracted to about 220 K for NNCS0, 240 K for NNCS1, 220 K for NNCS2, 200 K for NNCS3, and for 200 K NNCS4, while the P-R phase transition is recognized at 660 K for NNCS0, 640 K for NNCS1, 640 K for NNCS2, 600 K for NNCS3, and for 580 K NNCS4, respectively. It can be noted that the first-order P-R phase transition seems to present higher sensitivity with the content of $CaSnO_3$. In Fig. 4(b), NNCS100*x* ceramics go through phase transitions from P → HP-I → HP-II phase, where the HP-II phase is assigned to the paraelectric orthorhombic *Pbnm* phase as mentioned before. As for P to HP-I transformation, the pressure has the dominant effect on the interaction between Na^+ and NbO_6^- ions with NbO_6^- ions remaining octahedra. Otherwise, the distortion of NbO_6 octahedra, caused by further compression after touching of Na^+ and NbO_6^- ions, plays a dominant role under the high pressure condition. The $CaSnO_3$ content also reduces the critical pressure of phase transitions.

In conclusion, this work has systematically investigated the phonon dynamics, structure evolution, and the detailed phase diagrams of antiferroelectric (1-*x*)$NaNbO_3$-*x*$CaSnO_3$ ceramics under the control of temperature and pressure. Thermal induced successive phase transitions and two high-pressure phases are summarized in the phase

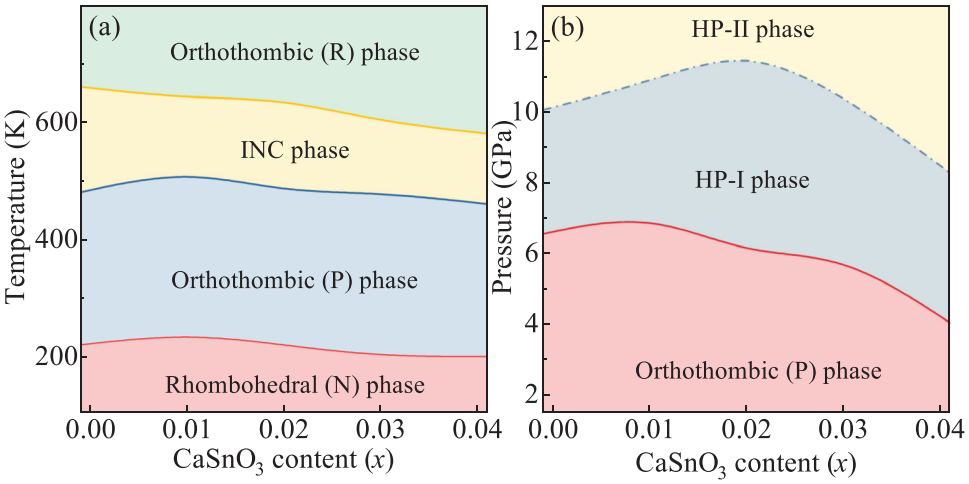

FIG. 4. (a) Temperature-dependent and (b) pressure-dependent phase diagram of NNCS100*x* ceramics with different $CaSnO_3$ contents.

diagram. The increasing substitution of the $CaSnO_3$ content reduces the temperature and pressure of the phase transition. Meanwhile, the INC phase during a high-temperature phase transition was identified at 480 K. The present study would pave the way to investigate more similar ferroelectric/antiferroelectric perovskite systems via Raman scattering in the future.

This work was financially supported by the National Natural Science Foundation of China (Grant Nos. 91833303, 61974043, 61805081, 62090013, and 12104156), the National Key Research and Development Program of China (Grant Nos. 2019YFB2203400 and 2017YFA0303403), Projects of Science and Technology Commission of Shanghai Municipality (Grant Nos. 18JC1412400, 18YF1407000, 18YF1407200, and 19511120100), the China Postdoctoral Science Foundation (Nos. 2020TQ0099 and 2020M681222), and the Program for Professor of Special Appointment (Eastern Scholar) at Shanghai Institutions of Higher Learning.

AUTHOR DECLARATIONS

Author Contributions

Y.Y. and A.C. contributed equally to this work.

DATA AVAILABILITY

The data that support the findings of this study are available from the corresponding author upon reasonable request.

REFERENCES

[1]C. Kittel, Phys. Rev. **82**, 729 (1951).
[2]D. Berlincourt, H. Jaffe, H. H. A. Krueger, and B. Jaffe, Appl. Phys. Lett. **3**, 90 (1963).
[3]A. S. Mischenko, Q. Zhang, J. F. Scott, R. W. Whatmore, and N. D. Mathur, Science **311**, 1270 (2006).
[4]M. M. Vopson, G. Caruntu, and X. Tan, Scr. Mater. **128**, 61 (2017).
[5]L. E. Cross, J. Phys. Soc. Jpn. **23**, 77 (1967).
[6]M. S. Mirshekarloo, K. Yao, and T. Sritharan, Appl. Phys. Lett. **97**, 142902 (2010).
[7]X. Tan, C. Ma, J. Frederick, S. Beckman, and K. G. Webber, J. Am. Ceram. Soc. **94**, 4091 (2011).
[8]D. Yang, J. Gao, L. Shu, Y.-X. Liu, J. R. Yu, Y. Y. Zhang, X. P. Wang, B.-P. Zhang, and J.-F. Li, J. Mater. Chem. A **8**, 23724 (2020).
[9]A. M. Glazer and K. Ishida, Ferroelectrics **6**, 219 (1973).
[10]R. A. Shakhovoy, S. I. Raevskaya, L. A. Shakhovaya, D. V. Suzdalev, I. P. Raevski, Y. I. Yuzyuk, A. F. Semenchev, and M. E. Marssi, J. Raman Spectrosc. **43**, 1141 (2012).
[11]J. Koruza, P. Groszewicz, H. Breitzke, G. Buntkowsky, T. Rojac, and B. Malic, Acta Mater. **126**, 77 (2017).
[12]A. Aydi, H. Khemakhem, C. Boudaya, and R. Mühll, Solid State Sci. **6**, 333 (2004).
[13]R. Z. Zuo, J. Fu, and H. Qi, Acta Mater. **161**, 352 (2018).
[14]J. M. Ye, G. S. Wang, X. F. Chen, F. Cao, and X. L. Dong, Appl. Phys. Lett. **114**, 122901 (2019).
[15]S. K. Mishra, N. Choudhury, S. L. Chaplot, P. S. R. Krishna, and R. Mittal, Phys. Rev. B **76**, 024110 (2007).
[16]S. K. Mishra, M. K. Gupta, R. Mittal, M. Zbiri, S. Rols, H. Schober, and S. L. Chaplot, Phys. Rev. B **89**, 184303 (2014).
[17]H. D. Megaw, Ferroelectrics **7**, 87 (1974).
[18]C. N. W. Darlington and K. S. Knight, Physica B **266**, 368 (1999).
[19]M. M. Shamin, T. Ishidate, and K. Ohi, J. Phys. Soc. Jpn. **72**, 551 (2003).
[20]S. E. Kichanov, D. P. Kozlenko, N. M. Belozerova, S. H. Jabarov, R. Z. Mehdiyeva, E. V. Lukin, A. I. Mammadov, H.-P. Liermann, W. Morgenroth, L. S. Dubrovinsky, B. N. Savenko, I. P. Raevskii, and N. T. Dang, Ferroelectrics **520**, 22 (2017).
[21]Z. X. Shen, X. B. Wang, M. H. Kuok, and S. H. Tang, J. Raman Spectrosc. **29**, 379 (1998).
[22]Y. Shiratori, A. Magrez, M. Kato, K. Kasezawa, C. Pithan, and R. Waser, J. Phys. Chem. C **112**, 9610 (2008).
[23]Y. I. Yuzyuk, P. Simon, E. Gagarina, L. Hennet, D. Thiaudière, V. I. Torgashev, S. I. Raevskaya, I. P. Raevskii, L. A. Reznitchenko, and J. L. Sauvajol, J. Phys.: Condens. Matter **17**, 4977 (2005).
[24]Y. Ye, A. Y. Cui, M. Y. Bian, K. Jiang, L. Q. Zhu, J. Z. Zhang, L. Y. Shang, Y. W. Li, Z. G. Hu, and J. H. Chu, Phys. Rev. B **102**, 024103 (2020).
[25]A. Y. Cui, X. H. Cao, Y. Ye, K. Jiang, L. Q. Zhu, M. H. Jiang, G. H. Rao, Y. W. Li, Z. G. Hu, and J. H. Chu, Phys. Rev. B **102**, 214102 (2020).
[26]Q. Q. Li, J. Y. Wang, M. J. Li, S. Guo, J. Z. Zhang, Z. G. Hu, Z. Y. Zhou, G. S. Wang, X. L. Dong, and J. H. Chu, Phys. Rev. B **96**, 024101 (2017).
[27]H. K. Mao, J. Xu, and P. M. Bell, J. Geophys. Res. **91**, 4673, https://doi.org/10.1029/JB091iB05p04673 (1986).
[28]A. C. Sakowski-Cowley, K. Lukaszewicz, and H. D. Megaw, Acta Cryst. **25**, 851 (1969).
[29]Y. Shiratori, A. Magrez, W. Fischer, C. Pithan, and R. Waser, J. Phys. Chem. C **111**, 18493 (2007).
[30]H. Guo, H. Shimizu, and C. A. Randall, Appl. Phys. Lett. **107**, 112904 (2015).
[31]L. Chao, Y. Hou, M. Zheng, and M. Zhu, Appl. Phys. Lett. **108**, 212902 (2016).